A Soil Vapor Extraction Pilot Study in a Deep Arid Vadose Zone Part 2: Simulations in Support of Decision Making Processes

P.H. Stauffer
Mail Stop T-003
Los Alamos National Laboratory
Los Alamos NM, 87545

J.K. Hopkins
Mail Stop M-992
Los Alamos National Laboratory
Los Alamos NM, 87545

T. Anderson
Apogen Technologies
1350 Central Ave.
Los Alamos NM, 87544

ABSTRACT

Soil vapor extraction (SVE) is a vital tool for remediating subsurface volatile organic plumes at waste sites with deep unsaturated zones. Plumes in the vadose zone are affected by many factors including vapor advection and diffusion, liquid movement, and source release processes. Leakage from buried drums may occur at different rates over the lifetime of a waste site, requiring modeling tools that can adequately address uncertain future scenarios. To demonstrate this concept, we present a numerical model of an SVE pilot test on a volatile organic compound (VOC) plume in the subsurface at Material Disposal Area L, Los Alamos National Laboratory. A site-scale numerical model was previously developed to evaluate the impact of subsurface processes on subsurface contaminants associated with waste disposed at the site. One important goal of model development is to support future corrective measures assessment activities. The model has been extensively tested and used to confirm our conceptual model for transport within the very dry mesa-top setting. In this study we present results of simulations of the SVE test. A 2-D radial model is used to test our conceptual model of flow and transport at this site. The 2-D model is calibrated to the SVE pilot test concentration and pressure data using field measured values for in situ permeability, porosity, saturation and site specific details such as asphalt coverage. A dual porosity formulation, including both matrix and fracture nodes, is necessary to fit the test data. Fracture flow at this site is necessary because the data show large drops in concentration from wells around the extraction hole that cannot be modeled as flow through a high porosity matrix. Matrix transport via diffusion into lower permeability storage provides a source term source that can replicate concentration rebound spike seen in data from the extraction borehole and other nearby boreholes. Simulations having matrix only are shown to fit the data at times greater than 3 weeks, suggesting that the matrix is strongly coupled to the fracture network and that dual porosity simulations may not be necessary for capturing long term behavior. Next we present a new high resolution, 3-D, site scale model that we plan to calibrated to the SVE pilot test concentration and pressure data using guidance from the 2-D radial model. We conclude by discussing how the 3-D model will be used to guide future decisions.

INTRODUCTION

Thousands of sites across the USA are contaminated with Volatile Organic Compounds (VOC) including trichloroethane (TCA), trichloroethene (TCE), and tetrachloroethene (PCE). These industrial solvents have high vapor pressure and low solubility and generally migrate faster in the vapor phase than in the liquid phase [1]. VOC plumes in the vadose zone can grow rapidly and are more likely to spread laterally because vapor diffusion is typically four orders of magnitude greater than liquid diffusion [2].

Remediation of vadose zone VOC plumes is required to protect human health, the environment, and deeper groundwater resources. VOC plumes in deep vadose zones rely on remediation techniques that differ substantially from techniques used to remediate plumes in the saturated zone. One of the primary remediation techniques currently used on VOC in the vadose zone is soil vapor extraction (SVE). SVE is appealing because of the relatively low costs associated with installation and operation, effectiveness of remediation, and widespread use at contaminated sites [3]. This technique uses an applied vacuum to draw pore gas toward an extraction hole. In a contaminated area, the extracted soil gas will contain some fraction of VOC in addition to air, water vapor, and CO2. As VOC is removed from the subsurface pore gas, any dissolved, adsorbed, or liquid phase VOC will tend to move into the vapor phase, thus reducing the total VOC plume [4]. Depending on the off-gas concentrations and local regulations, the gas stream may need to be treated by methods such as carbon adsorption or burning with a catalytic agent.

The most important factor in determining the effectiveness of an SVE system is the ability of the vapor-phase VOC to migrate toward the extraction well or wells [5]. Migration of VOC in the vadose zone can be impeded by high water saturation or very low intrinsic permeability. Vapor-phase relative permeability drops considerably as water saturation approaches the full porosity of the rock or soil [2]. Migration of VOC can also be impacted by the presence of high permeability conduits that allow advective transport to bypass lower permeability reservoirs of VOC. Such bypassing, or dual continuum behavior, can lead to much longer extraction times than predicted for a single permeability system because the VOC in lower permeability regions must diffuse to the advectively dominated regions before it can be extracted [6]. If the high permeability conduits lead to the atmosphere, a short circuit will be formed and will greatly reduce the extraction efficiency of SVE system. Low permeability wellbore skins can also lead to reduced extraction efficiency [5].

The focus of the current study is a VOC plume located in the vadose zone surrounding the primary liquid waste disposal area (MDA L) of Los Alamos National Laboratory (LANL). The plume is the result of leakage from a subsurface solvent landfill that received waste from 1975 – 1986 [7,8]. The vadose zone at this site is quite deep and SVE is being investigated as a possible corrective measure to remediate the plume. The initial investigation consisted of short duration (>30 days) SVE tests on two extraction holes that were designed to collect a range of data including pressure responses and concentration measurements from both the extraction holes and surrounding monitoring holes [8]. This paper describes the analysis of the data collected during the SVE pilot test. The analysis is performed using numerical methods that solve the coupled equations of gas flow and contaminant transport in porous media. We present results from a 2-D radial model of the site designed to allow confirmation of our conceptual model, then describe

preliminary results from a 3-D site scale model that has been built to predict site specific performance for a Corrective Measures Study.

SITE DESCRIPTION

Geology

Los Alamos National Laboratory is located on the Pajarito Plateau on the eastern flank of the Jemez Mountains. The Jemez Mountains were formed between 1 and 2 Ma with eruption of large volumes of ignimbrites [9]. The Pajarito Plateau is dissected by drainages resulting in narrow 'finger' mesas that are quite dry surrounded by wetter canyons. The most important rocks with respect to the current study are the ash-flow units 1 and 2 of Tshirege member of the Bandelier Tuff, Qbt1 and Qbt2 respectively. The uppermost unit at the site, Qbt2, is relative welded with ubiquitous vertical cooling joints. Many of the joints in this unit are filled with clay in the upper few meters, but are either open at depth, or filled with powdered tuff [10]. Qbt1 is subdivided into upper and lower units, Qbt1-v and Qbt-1g. Qbt1-v is subdivided into a non-welded upper unit and a welded lower unit, Qbt-1vu and Qbt-1vc respectively. Qbt-1vu is less welded than Qbt2 and has fewer cooling joints. Qbt-1vc is a welded tuff with many open vertical joints that provide rapid equilibration of pressure changes during pump tests [11]. Qbt 1g is a non-welded, glass bearing ash-flow that contains a few joints that appear to be continuations of joints formed in Qbt1-v that die out at depth. The basal unit of the Tshirege is the Tsankawi pumice (Qbt-t) that is very thin and probably discontinuous. Beneath the Tshirege is the Cerro Toledo (Qct), a volcanoclastic sediment interbedded with pyroclastic flows. Qct has fairly high permeability and porosity. Beneath the Qct is the Otowi member of the Bandelier Tuff, a poorly welded non-fractured ash-flow tuff. These units and their approximate distribution under MDA L can be seen in Figure 2 of Anderson [8]. For a more complete description of the geologic framework of the Pajarito Plateau, see Broxton and Vaniman [9]. MDA L is located at an elevation of 2073 masl (6800 ft), with an average atmospheric pressure of 80 kPa.

Vadose Zone Transport Properties

This section describes the physical properties that are relevant for the SVE modeling and is an expansion of properties discussed in Stauffer et al. [7] and references therein. Table I lists physical properties relevant for TCA transport. Table II lists the mean measured porosity, saturation, and effective diffusion coefficient determined from the best-fit model. Table III lists measured air permeability ranges for the geologic units beneath the site for both straddle packer measurements and core measurements. The straddle packer permeability measurements were made on seven boreholes directly to the East of MDA L. The packer interval was 0.6 m (2ft.) and the data provide a high resolution view of variability that is typical of the Bandelier Tuff. Straddle packer measurements were not made in the SVE boreholes used for the MDA L Pilot Test, thus the measured values provide the best initial guess as to the likely range of values expected around the SVE holes. The mean core permeability measurements are generally at least an order of magnitude lower than the mean straddle packer measurements, showing the role that fractures play in the rocks at MDA L. The permeability data show that increased

Table I 1,1,1-TCA Physiochemical Parameters

1,1,1-TCA ($C_2H_3CL_3$)	
Molecular weight [12]	133 g/mol
Liquid density [12]	1325 kg/m3 (at 293 K)
Vapor pressure [12]	100 mmHg (at 293 K)
Water solubility (mg/l) [12]	950 mg/L (at 293 K)
Tuff sorption coefficient K_d [13]	< 0.08 mL/kg fully saturated
Henry's Law constant (H_{TCA}) [14]	62 MPa/(liquid mole fraction) equal to 0.458 $(g/L)_{vapor}/(g/L)_{liquid}$ (at 285 K)
Diffusion coefficient in crushed Bandelier tuff assumed to be nearly equal to TCE $J = -\theta_a D \, gradC$ where J is flux, θ_a is volumetric air content, C is the concentration, and D is the diffusion coefficient. [15]	4.6 e-6 to 9.3 e-6 m^2/s at 2-7% relative saturation 4.4e-7 to 1.4e-6 m^2/s at 29-36% relative saturation

Table II Porosity, saturation, and effective diffusion coefficient values used in the simulations.

Unit	Effective porosity	In-situ saturation	D* (m^2/s)
Qbt 2	0.41[a]	0.06 [b]	$3x10^{-6}$
Qbt 1vu	0.49 [a]	0.15 [b]	$2x10^{-6}$
Qbt 1vc	0.49 [a]	0.15 [b]	$2x10^{-6}$
Qbt 1g	0.46 [a]	0.15 [b]	$2x10^{-6}$
Cerro Toledo	0.45 [a]	0.40 [b]	$5x10^{-7}$
Otowi Member	0.44 [a]	0.35 [b]	$5x10^{-7}$
Cerros del Rio basalt	0.1 [b]	0.02[c]	$3x10^{-6}$
Land surface	0.48 [c]	0.02 [c]	$3x10^{-6}$
Asphalt	0.5 [c]	0.02 [c]	$1x10^{-14}$
Shafts	0.5 [c]	0.02 [c]	$3x10^{-6}$
Wellbore	1.0	0.001	$3x10^{-6}$
Well Casing	0.5	0.001	$1x10^{-14}$

a fixed to mean measured value from Springer [16]
b fixed to measured values reported in Birdsell et al. [17]
c assigned fixed value for the simulations

Table III In situ and core permeabilty data for the MDA L area.

Geologic Unit	0.6 m Packer Permeability (m^2) Includes fractures [18]			Mean Core Permeability (m^2) Matrix only [16]
	MIN	MEAN	MAX	
Qbt 2	5.3e-13	1.7e-12	3.8e-12	2.0e-13
Qbt 1vu	4.7e-13	2.9e-12	1.6e-11	1.2e-13
Qbt 1vc	8.5e-14	1.5e-12	1.2e-11	1.2e-13
Qbt 1g	1.1e-13	2.5e-12	5.4e-11	1.3e-13
Qbtt	9.3e-13	7.5e-12	1.7e-11	NA
Qbct	1.2e-12	5.7e-12	1.1e-11	NA
Qbo	5.5e-13	6.1e-13	7.1e-13	2.3e-13[b]

b Canada del Buey data

permeability due to fractures at this site is not limited to the more welded Units Qbt-2 and Qbt-1vc, but is apparently ubiquitous throughout the Tshirege member of the Bandelier Tuff.

CONCEPTUAL MODEL

Processes included in the Conceptual Model

The conceptual model for plume growth at MDA L is described in Stauffer et al. [7], and we summarize the assumptions and findings of that study in this paragraph. These findings form the basis for the conceptual model used in the current paper. The primary VOC in the plume, comprising approximately 70% by mass of the total plume, TCA, is taken as representative of the plume. The VOC plume MDA L is controlled by vapor diffusion through variably saturated rocks with partitioning into the liquid phase. A zero concentration atmospheric boundary following the topography of the mesa and canyon is necessary to simulate the current plume. The rock saturation and porosity limit the ability of vapor to diffuse and the numerical representation of an effective diffusion coefficient are described below in the Model Formulation section. Henry's Law partitioning between the vapor and liquid phases (also described in the Model Formulation section) and greatly reduced diffusion across the asphalt at the site are both very important at MDA L. The best-fit land/air interface diffusion coefficient is slightly lower than the value used for the surface rocks, to represent the effects of a soil horizon that may contain more water than is found in the deeper mesa. Finally, the plume appears to be in a pseudo-steady state, growing only slowly, because most of the source release is following steep concentration gradients toward the atmosphere.

In this paper, we make the further assumption that during SVE, TCA transport can be described by the advection-dispersion equation. In addition to being a diffusive barrier, we assume that the asphalt has a low permeability. The role of fractures at this site may be quite important for simulating the SVE tests. Rocks containing fractures and porous rock matrix form a dual continuum that can behave differently than rocks containing only a single continuum of porous rock [6]. At this site, the rocks in Qbt2 and Qbt1-vc contain numerous vertical fractures that can lead to significant increases in permeability (Table III). Robinson et al. [19] found that water injection in the Bandelier Tuff showed behavior that was best fit with a single continuum representative of the matrix; however, air flow is substantially different from water flow due to capillary suction that pulls water into pores. Additionally, as described in the vapor transport section, the straddle packer data show much higher permeability than the core data for all units tested, therefore we explore the role of dual continuum behavior on the SVE system.

Processes not included in the Conceptual Model

Movement of liquid water at this site is assumed to be negligible (<1 mm/yr) and arguments for this assumption can be found in the conceptual model for flow and transport of liquid water beneath the Pajarito Plateau [20]. Additionally, temperatures vary only by a few degrees C within the region of interest in the mesa and we assume isothermal conditions for all simulations presented. Because measured effective diffusion coefficients of TCE on crushed tuff columns were very similar to those required to best fit the plume growth [15], we assume that barometric pumping within the mesa is not leading to increased apparent diffusion. Although the land/air interface in the previous model used a slightly lower effective diffusion coefficient, in the current model we do not reduce the permeability at this interface.

NUMERICAL MODEL

Model Formulation

We are using the Los Alamos porous flow simulator, FEHM, for all calculations presented in this paper [21]. FEHM is a finite-volume heat and mass transfer code that has been used extensively for simulation of multiphase transport [22, 23, 24, 25, 7, 26]. Equations governing the conservation of phase mass, contaminant moles, and energy are solved numerically using a fully implicit Newton-Raphson scheme. As stated in the conceptual model section, we simplify the analysis by assuming constant temperature and no movement of the liquid phase. Justification for these assumptions in the context of the Pajarito Plateau is given in Stauffer et al. [7]. Further, we assume that the atmospheric pressure is constant at 80 kPa.

The primary assumptions governing vapor-phase flow and transport are as follows. First, we assume that the vapor phase is composed solely of air that obeys the Ideal Gas Law and calculate vapor-phase density (kg/m^3) as a function of vapor pressure, P_v (MPa), and temperature, T (C) as:

$$\rho_v = 1.292864\left(\frac{273.15}{T+273.15}\right)\left(\frac{P_v}{0.101325}\right) \quad \text{Eq. 1}$$

We use Darcy's law to calculate the advective volume flux [27] of the vapor phase as:

$$v_v = -\frac{kR_v}{\mu_v}(\nabla P_v - \rho_v \bar{g}) \quad \text{Eq. 2}$$

where k is the intrinsic permeability of the rock (m^2), R_v is the relative permeability function for the vapor phase (calculated as a function of saturation via a Brooks-Corey relationship for this study [28]), $\bar{g}$ is the gravitational vector (9.81 m^2/s), and vapor viscosity is assumed constant as:

$$\mu_v = 1.82x10^{-5} Pa \cdot s \quad \text{Eq. 3}$$

Vapor-phase contaminant conservation is governed by the advection-dispersion equation (Fetter, 1999) where the contaminant flux (moles/(m^2 s))is given by:

$$q_v = v_v C_v + \phi S_v D^i{}_{cv} \cdot \nabla C_v \quad \text{Eq. 4}$$

where ϕ is porosity, S_v is vapor saturation defined as air filled porosity divided by total porosity, Cv is the molar concentration (moles/m$^3{}_{phase}$) and the dispersion coefficient, D_{cv}, includes contributions from both dispersivity and molecular diffusion as:

$$D^i{}_{cv} = \alpha^i v^i{}_v + D^*{}_v \quad \text{Eq. 5}$$

where the molecular diffusion coefficient in FEHM is a function of the free air diffusion coefficient (D_{free}) and the tortuosity (τ) as:

$$D^*_v = \tau D_{free}$$

Eq. 6

The dispersivity tensor (α^i) is directional; however in FEHM we keep only the diagonal terms of this tensor. The superscript i implies that the equation is solved for the principle directions. For example, in 3-D, the volume flux at any point can be decomposed into three principle components, ν_x, ν_y, and ν_z, while in 2-D radial the components are ν_r and ν_z. An additional constraint is imposed by Henry's Law equilibrium partitioning which requires a constant ratio between concentrations in the liquid and vapor phase as:

$$C_v = HC_l$$

Eq. 7

where the Henry's Law value for TCA (H_{TCA}) is listed in Table I. As described, the model is a molar based solution to the advection-dispersion equation using Fickian transport theory. We do not account for the effects of non-Fickian diffusion; however corrections for non-equimolar behavior are relatively small (<3%) [29].

Another key feature of FEHM is the generalized dual continuum method (GDPM) that allows simulation of fracture/matrix interactions. For this formulation, each node of the primary grid is assigned fracture properties. Each fracture node is assigned a fraction that specifies what percent of the total cell volume is occupied by the fracture. The remaining volume is divided into any number of matrix nodes that are coupled to the fracture node through the flow and transport equations in one dimension. The matrix nodes are not part of the primary grid and matrix nodes associated with different primary nodes are not connected to each other. Thus, the matrix nodes in this formulation act as storage for liquid and vapor mass that can move into and out of the matrix driven by either gradients in pressure or gradients in concentration. The GDPM function has been extensively tested and used to simulate heterogeneous DNAPL migration [30].

2-D Model Domain and Computational Grid

Initial calculations for this project were performed on a 2-D radial grid. Because of limitations of the 2-D representation, the grid is designed to capture the basic configuration of the site. In such a system, the finger mesa can be approximated as a right circular cone. The borehole is located at the center of the right circular cone-mesa (Figure 1a). The domain is 120 m high by 150 meters wide. The radius of the flat top cone 'mesa' is 50 m. The slope leading from the mesa top to the canyon below drops 35.5 m vertically over a radial distance of 50 m. These values are based on the topography found to the north of MDA L where Mesita del Buey slopes down into Canada del Buey. The grid has 41693 primary nodes with a constant spacing of 0.5 m in the vertical direction and variable spacing in the radial direction. The first two nodes in the radial direction are located within the borehole radius (0.0794 m). The nodes outside of this radius increase in spacing until r > 3 m when spacing is fixed at 1 m to edge of the grid at r = 120m. The 2-D grid contains a highly permeable borehole with suction applied at the top and casing modeled as a very low permeability skin around the flowing hole. This configuration allows the applied suction to extract subsurface pore gas from the appropriate units based on the distribution of permeability that is specified. The cased and open sections of the borehole with

respect to the numerical grid are shown in Figure 1a. More discussion of the borehole construction can be found in Anderson et al. [8].

The boundary conditions on the 2-D domain include a single node of fixed pressure at the top of the extraction borehole (66.8 kPa), no flow along the bottom of the grid, and fixed atmospheric pressure (80 kPa) along the atmospheric boundary and along the r=150 m boundary (shown as bright green lines on Figure 1). Temperature throughout the domain is fixed at 15 C for all simulations based on temperature data from the experiment. Because the extraction forces are much greater than gravitational forces, we have removed gravity from the solution by setting $\bar{g}$ = 0 in Equation 2. At the top of the extraction borehole, the air density is 0.81 kg/m3, leading to calculated mass removal based on concentration measurements in parts per million by volume (ppmv) to be significantly different than one would calculate using standard PT conditions where the number of moles of air in a given volume is nearly 50% greater.

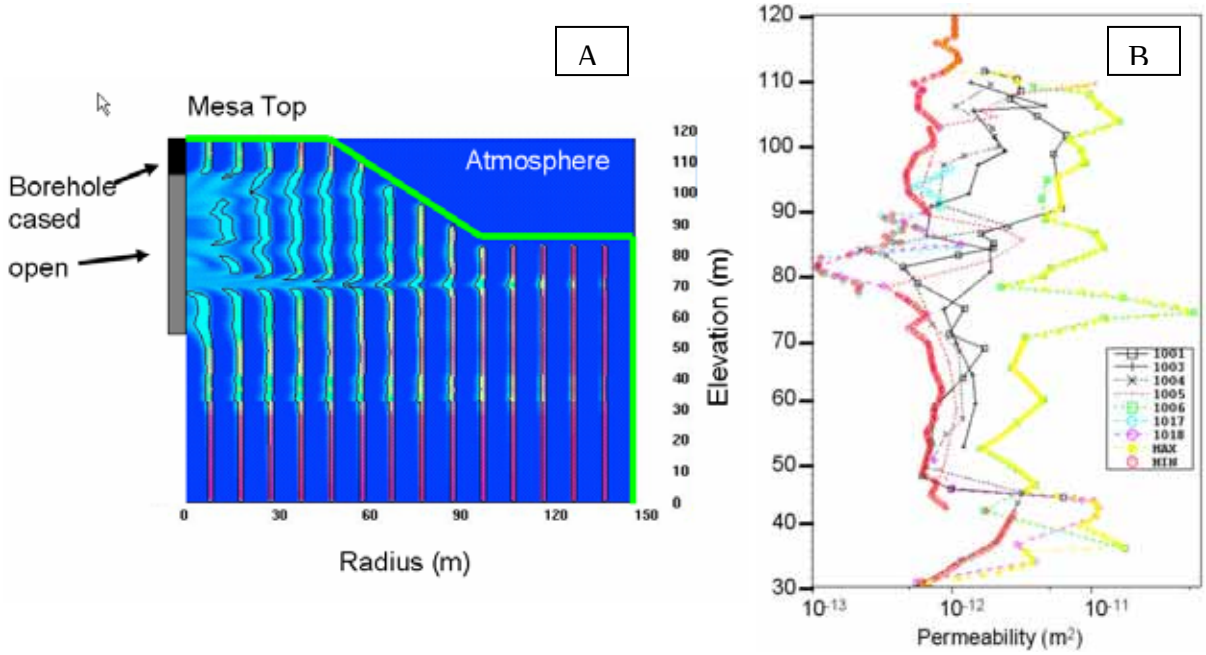

Figure 1 a) 2-D radial domain with an example simulation using the MAX permeability curve shown in b) downhole straddle packer data for several boreholes to the east of MDA L.

Effects of dispersivity on the 2-D grid were examined by varying the hydrodynamic dispersivity term (Eq. 5) from zero until changes were seen in the calculations. From this exercise we determined that numerical dispersion associated with the 2-D radial grid at the flow rates we are simulating is on the order of 1-2 m. Vapor-phase dispersivity in the unsaturated zone is poorly documented [31]. Because true vapor velocities toward the borehole are only high within 10-20m, meaning that the flow path length is of the same order, rough estimates based on water behavior where longitudinal dispersivity scales as approximately as 1/10 of the flow path would suggest that an appropriate value for our system would be between 1-2 m [2]. Therefore we have chosen to set all components of the hydrodynamic dispersion tensor (α^{rz}) to zero, thus our simulations include only the effects of numerical dispersion with an effective $\alpha^{r} = \alpha^{z} = 1$ m.

3-D Model Domain and Computational Grid

Numerical Grid

The 3-D simulation domain is approximately centered on MDA L, and includes the surrounding mesa/canyon environment from the land surface to the water table. Figure 2 shows a portion of the computational domain with several relevant boreholes labeled, the site boundary as a heavy black polygon, and an orthophoto showing roads and buildings. A more detailed map of MDAL can be found in Figure 1 of Anderson [8]. MDA L is approximately 180 m E-W by 120 m N-S (600 x 400 ft), and the simulated domain extends beyond the site on all sides by a minimum of 100 m to minimize boundary effects. The computational grid is made up of over 140,000 nodes and nearly 800,000 volume elements. The lateral extent is 410. m E-W by 370 m N-S. The grid extends vertically from an elevation of 1737 meters above sea level (masl) at the water table to 2074 masl on the northwestern corner of Mesita del Buey. The grid has a vertical resolution of 1 m in the top 90 m and stretches to a resolution of 25 m at the water table. The horizontal resolution is everywhere 10 m in both x and y. The grid captures the topography of the site and extends to the water table, over 300 m below the surface of the mesa on which MDA L is situated. The deeper part of the grid, 270 ft (90 m) below the mesa top, has little impact on the simulations, and is included with a vertical spacing of 10 m to address questions concerning plume impacts on the regional water table. The 3-D grid used in this paper is an extension and refinement of the grid used in Stauffer et al. [7] and images from that paper will be helpful for the reader to visualize the current domain and grid.

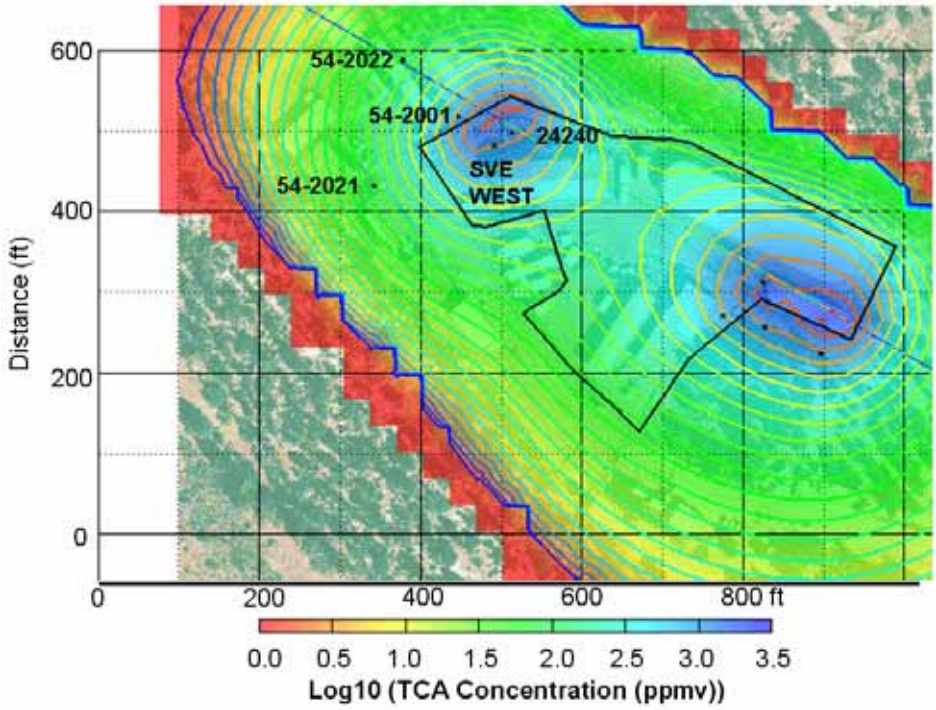

Figure 2 Initial condition of the3-D SVE model on a slice plane 60 ft (18.3 m) below the top of the SVE West well.

Wellbore Capability

FEHM has a new capability that allows us to embed radial boreholes within an existing 3-D site scale mesh [32]. This capability is used to reduce the total number of nodes required to capture the radial flow near the simulated SVE extraction holes while also capturing the topography and stratigraphy at the site scale. Without this capability, we would have had to embed two 3-D extraction borehole meshes and all the necessary extra nodes to allow the borehole meshes to correctly connect to the existing 3-D grid while maintaining the Voronoi volume constraints that are required for computational accuracy. Furthermore, the flexibility allowed by the new capability is such that one can add or remove boreholes at any time, permitting us to study the effects of SVE borehole placement location without having to spend large amounts of time embedding 3-D borehole meshes into site scale grids. The wellbore capability includes the ability to add onion shells around the open hole. The wellbores used in the simulations each have an inner radius of 0.08 m and an outer shell radius of 2 m with 4 nodes spanning this distance. Therefore each well has one vertical line of nodes representing the open hole and four onion skins surrounding this. Both SVE holes have a total depth of 66 m with 67 nodes along the vertical. The nodes representing the open hole are assigned a permeability of 5×10^{-7} m^2, providing little resistance to flow in the open hole. The first onion skin in the upper 20 m of each hole are assigned a permeability of 5×10^{-19} m^2 and a diffusion coefficient (D*) of 5×10^{-19} m^2/s to simulate the effects of the steel casing. Nodes in the second and third onion skins are assigned the rock and tracer properties specified in a given simulation for the geologic unit in which they reside. Currently, use of the wellbore module precludes the use of GDPM; however, we are working to allow simultaneous use of both options in the near future.

RESULTS AND DISCUSSION

All simulations presented in this paper focus on the first 22.9 days of the West SVE Pilot test. This time period allows us to test the conceptual models of flow at the site, while reducing simulation time and effort.

Pretest 2-D Simulations

We first present a generic simulation of flow in a stratified variable permeability system. Figure 1 shows the results of extraction simulations that were done using the pre-test high permeability estimate from the straddle packer data. Figure 1 is designed to allow visualization of the movement of a hypothetical tracer in response to extraction of 2.69 m^3/min (95 ft^3/min) from to the top of the borehole. The image was created by initializing the domain with a gas phase tracer of concentration 1.0 mol/kg_{air} in narrow vertical bands spaced along the radius of the domain. The bands of tracer, initially red, become smeared and stretched as they are pulled toward the open interval of the borehole. The high permeability estimate was generated by taking the highest measured value over each 0.67 m (2 ft) depth interval and setting a layer of rock to this permeability (see Figure 4; Neeper, 2002). A particularly narrow band of high permeability can be seen at z = 70 m with effects of the SVE seen at distances of greater than 90 m (295 ft), a result that contrasts with simple pretest estimates of 140 ft (43 m) for the radius of influence. Suction versus flow rate was computed for two end member permeability distributions based on the 0.67 m packer data. Data from the SVE West test fell nearly on the extraction versus suction line from the high permeability case showing that the downhole bulk permeability is at least an order of magnitude greater than the measured core permeability. Because the bulk permeability

that is required to match the test data lies well above the values measured on core, the downhole permeability at this site most likely includes the effects of many fractures throughout the section.

Calibration of the 2-D model to the SVE West Test

The 2-D domain was initialized with a concentration profile based on data from a monitoring well located approximately 8m from the SVE West hole. This profile was chosen to give a rough estimate for the initial concentrations near the extraction hole. The model was run with diffusion only (v=0 in Eq. 5) with points around the borehole to r = 11m fixed at the concentrations suggested by the nearby borehole. This resulted in a plume of approximately 540 kg TCA in the initial domain partitioned between the vapor phase and the dissolved phase. A range of simulations were performed to determine the behavior of the simulated vapor extraction and simulated values of concentration at points corresponding to monitoring wells near the extraction hole. While attempting to calibrate the model to the extraction data (Figure 3a), the permeability of individual units was varied in both the radial and vertical directions. Additionally, we varied parameters in a thin high permeability horizon that was placed in the model space from z=95.5 m to z=101.5 m based on a consistently low observed manometer reading at this depth in a well 24240 which can be seen in Figure 4 of Anderson [8]. Because the model is run with a fixed pressure at the top of the extraction borehole (66.8 kPa), any changes to unit permeabilities needed to be balanced so that the net extraction remained very near the test average extraction of 2.63 m^3/min (95 ft^3/min). The West test was initiated on June 14th and finished on July 7th 2006, with a brief 4 day hiatus in extraction due to failure of a pulley mechanism on the extraction pump.

Figure 3a shows a plot of the concentration at the top of the extraction well versus time for both data and modeling results. We first calibrated the SVE extraction concentration for a dual

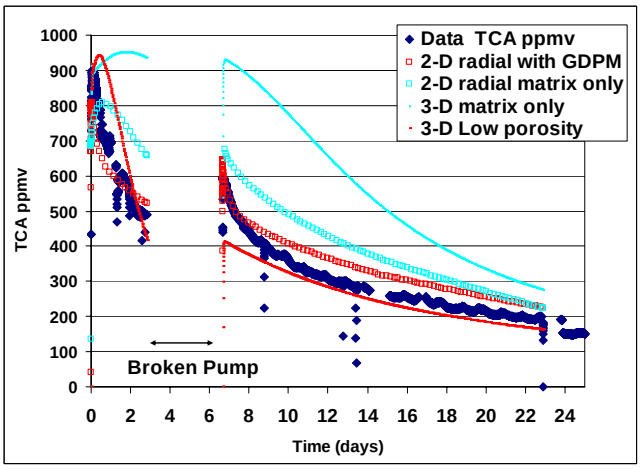

Figure 3 Model results compared to test data with: A) TCA concentration versus time in the SVE West extracted gas stream and B) cumulative TCA mass removed versus time. Time equal zero is the start of the SVE West test. The four day data gap was caused by pump failure.

porosity system with high porosity in the matrix material and high permeability in a fracture continuum. Each matrix volume attached to a primary fracture node has four nodes that span the volume. The total volume of each fracture is 0.001 times the volume of the original finite volume element, meaning that the matrix in this example is comprises of 99.9% of the subsurface. Permeabilities used in this simulation are given in Table IV.

Table IV Permeability and porosity used in the simulations.

Unit	2-D Fracture permeability m^2		2-D Matrix permeability m^2		3-D Matrix permeability m^2	
	r	z	r	z	x and y	z
Qbt 2	1.0e-11	4.0e-11	1.0e-11	4.0e-11	5.0e-12	5.0e-12
Qbt 1vu	1.0e-11	4.0e-11	1.0e-11	4.0e-11	4.0e-12	1.0e-11
Thin high perm unit	1.5e-11	3.0e-11	1.5e-11	3.0e-11	2.0e-11	2.0e-11
Qbt 1vc	5.0e-12	1.0e-11	5.0e-12	1.0e-11	1.0e-12	1.0e-12
Qbt 1g	2.0e-12	2.0e-12	2.0e-12	2.0e-12	7.0e-13	7.0e-13
Tsankowi pumice	6.0e-12	6.0e-12	6.0e-12	6.0e-12	3.5e-12	3.5e-12
Cerro Toledo	6.0e-12	6.0e-12	6.0e-12	6.0e-12	1.0e-12	1.0e-11
Otowi Member	6.0e-13	6.0e-13	6.0e-13	6.0e-13	3.5e-13	3.5e-13
Asphalt	5.0e-19	5.0e-19	5.0e-19	5.0e-19	1.0e-16	1.0e-16
Wellbore	8.0e-8	8.0e-8			5.0e-7	5.0e-7
Well Casing	5.0e-19	5.0e-19	5.0e-19	5.0e-19	5.0e-19	5.0e-19

On Figure 3a, this simulation is labeled '2-D radial with GDPM' and exhibits behavior that is similar to the experimental data. The initial concentrations in the extraction stream are quite high and drop quickly during the first 2.9 days of the test. Furthermore this simulation is able to recreate the rebound spike seen in the data at 6.6 days. The rebound spike occurred during an unplanned pump failure and the extra data the failure provided was instrumental in forming our conceptual model for dual continuum transport. Figure 3b confirms that the total amount of TCA removed during this simulation is nearly equal to the amount removed during the test. Figures 4a and 4b show a comparison between the model and test data for TCA concentration in borehole 24240 (see Figure 2 for location) at depths of 50 and 100 ft (15.24 and 30.48 m) below

the surface. These plots are not meant to exactly match the data because the 2-D simulations are a simplification of the real system, with the plume centered on the extraction hole and only a rough estimate of the initial concentration profile. The simulation was not calibrated to the data at this location; however the character and general magnitude of the simulation is remarkably similar. The initial concentration at both depths drops sharply until the pump failure at which time a rebound is observed. After the pump was restarted at 6.6 days, the concentration in the monitoring well continues to drop with the slope gradually decreasing as if the concentrations were approaching an asymptotic value of perhaps 100 ppmv.

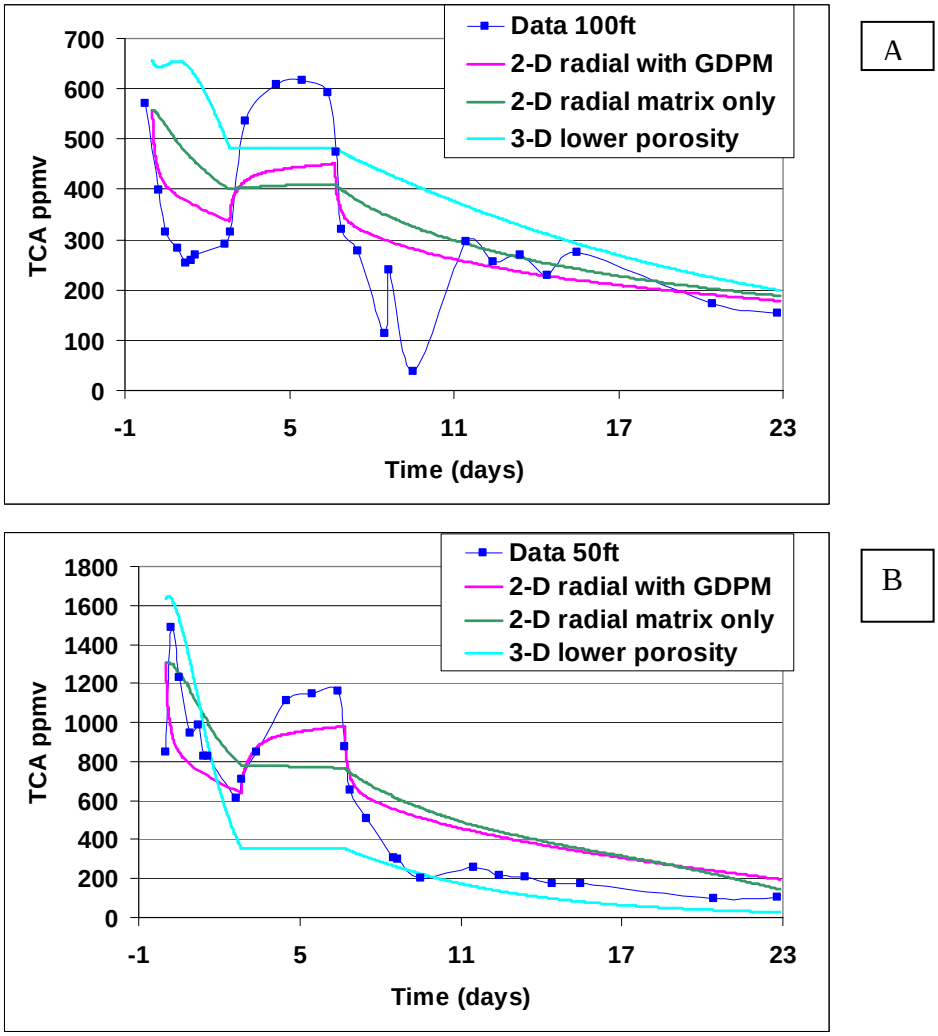

Figure 4 Model results compared to data in borehole 24240 at depths of a) 50 ft and b)100 ft Time equal to zero is the start of the SVE West test.

The model curve labeled '2-D radial matrix only' in Figures 3 and 4 shows the results for a simulation that includes only matrix material. The simulation uses the same permeabilities in the entire matrix that were used for the 2-D GDPM fractures in the simulation presented above. The simulated concentrations at early times are close to the data, but at longer times the simulation is unable to recreate the sharp drop in concentration seen in the data. This simulation also does not recreate the rebound spike seen in the data at 6.6 days. Interestingly, at later times this

simulation reaches about the same concentration as the GDPM simulation. This may mean that the matrix component of the dual continuum is well connected and that the system can be modeled essentially as a single continuum for simulations that examine SVE implementation over the span of years. Part of our ongoing research is to determine how important the matrix storage component is at this site, and on what time scales it operates. Further analysis will include examining the long term rebound over the next few months at boreholes surrounding the SVE boreholes. Another process that could be contributing to the rebound seen both during the pump failure and in post-test modeling is rate limited equilibration of vapor and liquid phases. Huang and Goltz [33] note that laboratory results for a range of contaminants show rate limited sorption and phase transfer. Such behavior would closely mimic the effects of matrix diffusion, providing a time dependent source of contaminant. At MDA L the most likely rate limiting process would be the equilibration from dissolved VOC into the soil gas. Because this simulation does not reproduce the correct concentration in the extracted gas, the mass removal rate plot (Figure 3b) is also not correct. The simulated concentrations in wellbore 24240 are relatively close to the data but the simulation is unable to reproduce the rebound spike (Figure 4a and 4b).

3-D Simulations: Boundary and Initial Conditions

All 3-D simulations include an extraction wellbore as described above, labeled as 'SVE West' on Figure 2, with a borehole radius of 7.94 cm (3.125 inches) and 4 additional nodes reaching 2 m radially from the borehole to capture the radial flow toward the borehole from the surrounding volume elements. The wellbore reaches from the surface to a depth of 65 m (215 ft) and has vertical resolution of 1 m. The permeability distribution used in the 2-D simulations where applied to all of the 3-D simulations. The domain was initialized with concentrations in the source region fixed to values representing the maximum observations and the two source regions were activated at the appropriate time from 1975 until 2006 (see Stauffer et al. [7] for a more thorough explanation of the plume generation algorithm). The initial concentration of TCA on a plane at a depth of 60 ft (20 m) below the surface is shown on Figure 2. From this figure one can see the intersection of the plume with the atmosphere at the canyon slopes, where the plume delineates the narrow finger mesa on which MDA L is situated. The total width of the mesa at this location is only approximately 500 ft (152 m). The source locations in this higher resolution grid are modified slightly from Stauffer et al. [7], and the new simulation results for 2006 were compared to the data from the previous modeling combined with new data collected during the past few years. The model-data regression remained quite good with an r^2 correlation coefficient of greater than 0.89. Therefore we are confident that the initial condition for the 3-D SVE simulations is a very good representation of the actual plume beneath MDA L.

3-D Simulation Results

In this section we discuss the preliminary calibration results for the 3-D model. Figures 3a and 3b include results from a simulation that uses the 3-D grid in which permeabilities were set to the values reported in Table IV, labeled '3-D matrix only'. Pressure was maintained at 66.8 kPa at the top of the extraction hole, and changes in concentrations through time in the extracted gas are plotted against the data. The initial concentrations at this location are much higher than in the 2-D simulations. This is mainly due to the fact that the initial condition in this example is closer to the in situ plume. The single continuum results show no rebound spike, but appear to be trending toward an asymptote at the 200 ppmv level by 22 days.

A final simulation is presented in which the 3-D simulation porosity was reduced to mimic the effects of a dual continuum simulation on short time scales. This curve is labeled '3-D lower porosity' on Figures 3 and 4. The initial drop in concentration in the extracted gas for this example is much closer to the data but there is no rebound because there is no matrix storage. After 6.6 days, porosity was increased to mimic the conceptual model that the matrix is equilibrating by this time, and the resulting curve lies fairly close to the data. Simulated concentrations at borehole 24240 also recreate the data fairly well.
The 3-D simulations presented in this paper are preliminary in the sense that the model still needs to undergo a significant amount of calibration to additional data such as the longer time history after the testing ended, the manometer data, and data from more monitoring boreholes both during and after the completion of the SVE testing. The simulations presented give a good initial estimate of the behavior of SVE at this site and further work will permit the model to be used in the design and implementation of possible remediation alternatives.

CORRECTIVE MEASURES STUDY APPLICATIONS

One of the primary recommendations of the MDA L RFI report [34] was that a corrective measures study should be performed at this site. In this section we discuss how the results from the modeling will be used to guide decisions about possible remediation alternatives. Once the 3-D model has been more fully calibrated to the SVE Pilot Test data, we plan to use the model to explore scenarios that are relevant to choosing a corrective measure at MDA L.

First, the simulations will be used to test the effectiveness of the VOC extraction process over longer times than were allowed during the brief pilot test. Determining the time required to extract a significant proportion of the plume is vital to making estimates of remediation costs. A simulated extraction study will also determine which monitoring points are the most useful and what frequency of monitoring is required to ensure that changes to the plume can be seen in the monitoring data.

Second, the simulations can be modified to work with a variety of corrective measures alternatives. For example, we can include various cover designs to test the effect of implementation on the proposed SVE system. Previous modeling showed that the presence asphalt at this site will lead to a larger plume for a given source strength (Stauffer et al. 2005). The current modeling has also provided insight that suggests an impermeable barrier will cause the vapor extraction pump to pull air from deeper within the mesa. By understanding the way the SVE process interacts with the asphalt, covers, and rocks of the mesa, we will be able to create a more effective remediation plan with respect to action levels, costs, and clean-up time.

The third and perhaps most important use of the modeling will be to show how an SVE system could be used at MDA L to respond to catastrophic failure of drums containing VOC. In this modeling demonstration we plan to estimate the time required to detect a catastrophic failure using the in-situ monitoring network. Knowing how long it will take to detect such a failure will allow implementation of a sampling plan to maximize the 'early warning' capability of the monitoring network, either by suggesting new monitoring ports or showing which of the existing ports are most useful for early detection. We envision that the early warning design can provide

data for a decision point that can trigger activation of the SVE system if action levels are exceeded. Under this plan, the SVE system will not need to be run constantly, but will used as an auxiliary intervention device when needed. We will also use the model to show the effectiveness of the SVE system to remediate any VOC released during such a hypothetical catastrophic event. We believe that the modeling will show that, even in extreme release scenarios for this site, SVE technology can be used successfully to extract the increased VOC load and stop any migration toward the regional water table. We must stress that modeling is the only tool available to explore catastrophic failure and the model results can be used in demonstrating to Stakeholders that the proposed closure plan is comprehensive and safe.

CONCLUSIONS

Data collected during a one month SVE test are sufficient to calibrate a site-scale 3-D model of VOC transport at MDA L. Simulations using both a 2-D radial grid and the full 3-D site scale model shows that dual continuum behavior is necessary to fit the extraction versus time profile in the extracted stream, as well as to fit the concentration rebound seen in nearby monitoring wellbores. The simulations show that the effect of matrix storage is more pronounced at time scales of less than a week; however the matrix storage may have enough communication with the fracture network so that on time scales of greater than a few weeks, the system may respond more like a single continuum. We plan to continue to study the dual continuum nature of this system to better characterize this preliminary result. Finally, the calibrated model will be useful in answering questions related to long term stewardship at this site. Specifically the simulations will be used to optimize the monitoring network, examine effects of cover design on SVE performance, and study how SVE may be an effective tool in remediating hypothetical catastrophic releases at this site. Preliminary simulations of the extraction processes show that SVE will be a very effective remediation tool at this site.

REFERENCES

1. W.A. Jury, D. Russo, G. Streile, and H. Abd, "Evaluation of Volatilization by Organic Chemicals Residing Below the Soil Surface", Water Resour. Res. 26:13-20 (1990).

2. C.W. Fetter, Contaminant Hydrogeology, Prentice-Hall, NJ, USA (1999).

3. J.H. Lehr, Wiley's Remediation Technologies Handbook, Major Contaminant Chemicals and Chemical Groups, John Wiley and Sons, Hoboken NJ (2004).

4. S. Hoeg, H.F. Scholer, and J. Warantz, "Assessment of interfacial mass transfer in water-unsaturated soils during vapor extraction", J. of Contaminant Hydrology 74:163-195 (2004).

5. G.C. Bradner and L.C. Murdoch, "Effects of skin and hydraulic fractures on SVE wells", J. of Contaminant Hydrology 774:271-297 (2005).

6. K. Preuss and J.S.Y. Wang, "Numerical Modeling of Isothermal and Nonisothermal Flow in Unsaturated Fractured Rock: A Review", in Flow and Transport Through Unsaturated Fractured Rock, Second Edition, Geophysical Monograph 42, eds. D.D. EVANS, T.J. NICHOLSON, and T.C. RASMUSSEN, AGU, Washington D.C. (2001).

7. P.H. Stauffer, K.H. Birdsell, M.S. Witkowski, and J. K. Hopkins, "Vadose Zone Transport of 1,1,1-Trichloroethane: Conceptual Model Validation through Numerical Simulation", Vadose Zone Journal 4(3): 760-773 (2005).
8. T. Anderson, "A Soil Vapor Extraction Pilot Study in a Deep Arid Vadose Zone, Part I", WM Symposium Proceedings, this volume (2007).
9. Broxton D.E., and D.T. VANIMAN, "Geologic Framework of a Groundwater System on the Margin of a Rift Basin, Pajarito Plateau, North-Central New Mexico", Vadose Zone Journal 4(3):522:550 (2005).
10. D.A. Neeper and R.H. Gilkeson, "The influence of Topography, Stratigraphy, and Barometric Venting on the Hydrology of Unsaturated Bandelier Tuff", New Mexico Geological Society Guidebook, 47th Field Conference, Jemez Mountains Region, pp. 427-43 (1996).
11. D.A. Neeper, "Investigation of the vadose zone using barometric pressure cycles", J. of Contaminant Hydrology 54, 59–80 (2002).
12. A.D. Little, "The Installation Restoration Program Toxicology Guide", 1:1–16 (1987).
13. S.K. Ong and L.W. Lions, "Effects of soil properties and moisture on the sorption of trichloroethylene vapor", Water Res. 25: 29–36 (1991).
14. R. Sander, "Henry's Law Constants" in NIST Chemistry WebBook, NIST Standard Reference Database Number 69, P.J. Linstrom and W.G. Mallard (ed.), National Institute of Standards and Technology, Gaithersburg MD (2003).
15. H.R. Fuentes, W.L. Polzer, and J. L. Smith. "Laboratory Measurements of Diffusion Coefficients for Trichloroethylene and Orthoxylene in Undisturbed Tuff", J. Environ. Quality, 20:215-221 (1991).
16. E.P. SPRINGER, "Statistical Exploration of Matrix Hydrologic Properties for the Bandelier Tuff, Los Alamos, New Mexico", Vadose Zone Journal 4:505-521 (2005).
17. K.H. Birdsell, A.V. Wolfsberg, D. Hollis, T.A. Cherry, and K.M. Bower, "Groundwater Flow and Radionuclide Transport Calculations for a Performance Assessment of a Low-Level Waste Site", J. of Contaminant Hydrology 46:99-129 (2000).
18. D.B. Rogers and B.M. Gallaher, "The unsaturated characteristics of the Bandelier Tuff", Los Alamos National Laboratory Report, LA-12968-MS (1995).
19. B.A. Robinson, S.G. Mclin, and H.S. Viswanathan, "Hydrologic Behavior of Unsaturated, Fractured Tuff: Interpretation and Modeling of a Wellbore Injection Test", Vadose Zone Journal 2005 4(3):694-707 (2005).
20. K.H. Birdsell, B.D. Newman, B.A. Robinson and D.E. Broxton, "Validation of the Conceptual Model for Vadose-Zone Flow and Transport beneath the Pajarito Plateau, Los Alamos, New Mexico", Vadose Zone Journal, 4:620-636 (2005).
21. G.A. Zyvoloski, B.A. Robinson, Z.V. Dash, and L.L. Trease, "Summary of the models and methods for the FEHM application-a finite-element heat-and mass-transfer code", Los Alamos National Laboratory report, LA-13307-MS (1997).

22. P.H. Stauffer, L.H. Auer, and N.D. Rosenberg, "Compressible gas in porous media: A finite amplitude analysis of natural convection", Int. J. of Heat and Mass Transfer, 40 (7), 1585-1589 (1997).

23. P.H. Stauffer and N.D. Rosenberg, "Vapor phase transport at a hillside landfill", Environmental and Engineering Geoscience, Vol. VI, No. 1, p. 71-84 (2000).

24. A.V. Wolfsberg and P.H. Stauffer, "Vadose-zone fluid and solute flux: advection and diffusion at the Area 5 Radioactive Waste Management Site", Los Alamos National Laboratory Report, LA-UR-03-4819 (2004).

25. D.A. Neeper and P.H. Stauffer, "Unidirectional gas flow in soil porosity resulting from barometric pressure cycles", J. of Contaminant Hydrology, 78(4), 281-289 (2005).

26. E.M. Kwicklis, A.V. Wolfsberg, P.H. Stauffer, M.A. Walvroord, and M.J. Sully, "Multiphase Multicomponent Parameter Estimation for Liquid and Vapor Fluxes in Deep Arid Systems Using Hydrologic Data and Natural Environmental Traces", Vadose Zone Journal, 5:934-950 (2006).

27. P.H. Stauffer, "Flux Flummoxed: A Proposal for Consistent Usage", Ground Water, 44(2): 125-128 (2006).

28. R.H. Brooks and A.T. Corey, "Properties of porous media affecting fluid flow", Proceedings, American Society of Civil Engineers, Irrigation and Drainage Division 92(IR2):61-87 (1966).

29. C.S. Fen and L.M. Abriola, "A comparison of mathematical formulations for organic vapor transport in porous media", Advances in Water Resources, 27:1005-1016 (2004).

30. D. Rodriguez, "Significance of Diffused Zone Mass Flux Plumes in Determining the Longevity of Solute Plumes Emanating From Heterogeneous DNAPL Source Zone" Ph.D. Dissertation , Colorado School of Mines (2006).

31. T.D. Gidda, D. Cann, W.H. Stiver, and R.G. Zytner, "Airflow dispersion in unsaturated soil", J. Contaminant Hydrology, 82(1), 118-132 (2006).

32. R.J. Pawar and G.A. Zyvoloski, "A Novel Method to Couple Wellbore Flow to Reservoir Flow", in Proceedings of the XVI International Conference on Computational Methods in Water Resources, edited by P.J. Binning, P.K. Engesgaard, H.K. Dahle, G.F. Pinder and W.G. Gray, Copenhagen, Denmark, June, (2006).

33. J. Huang and N.G. Goltz, "Solutions to equations incorporating the effect of rate-limited contaminant mass transfer on vadose zone remediation by soil vapor extraction", Water Resources Research 35(3):879-883 (1999).

34. LANL, "RCRA Facility Investigation Report, Los Alamos National Laboratory, Material Disposal Area L at Technical Area 54", LANL publication LA-UR 02-7803 (2003).